Hydrol. Earth Syst. Sci. Discuss., 9, 6615–6647, 2012
www.hydrol-earth-syst-sci-discuss.net/9/6615/2012/
doi:10.5194/hessd-9-6615-2012


Hydrology and Earth System Sciences Discussions



# Deriving global flood hazard maps of fluvial floods through a physical model cascade

**F. Pappenberger**[1,2], **E. Dutra**[1], **F. Wetterhall**[1], **and H. Cloke**[1,3]

[1]European Centre for Medium Range Weather Forecast, Reading, UK
[2]Hydrology and Water Resources, Hohai University, Nanjing, China
[3]Department of Geography, King's College London, London, UK

Received: 10 May 2012 – Accepted: 17 May 2012 – Published: 25 May 2012

Correspondence to: F. Pappenberger (florian.pappenberger@ecmwf.int)

Published by Copernicus Publications on behalf of the European Geosciences Union.







## Abstract

Global flood hazard maps can be used in the assessment of flood risk in a number of different applications, including (re)insurance and large scale flood preparedness. Such global hazard maps can be generated using large scale physically based models of rainfall-runoff and river routing, when used in conjunction with a number of post-processing methods. In this study, the European Centre for Medium Range Weather Forecasts (ECMWF) land surface model is coupled to ERA-Interim reanalysis meteorological forcing data, and resultant runoff is passed to a river routing algorithm which simulates floodplains and flood flow across the global land area. The global hazard map is based on a 30 yr (1979–2010) simulation period. A Gumbel distribution is fitted to the annual maxima flows to derive a number of flood return periods. The return periods are calculated initially for a 25 × 25 km grid, which is then reprojected onto a 1 × 1 km grid to derive maps of higher resolution and estimate flooded fractional area for the individual 25 × 25 km cells. Several global and regional maps of flood return periods ranging from 2 to 500 yr are presented. The results compare reasonably to a benchmark data set of global flood hazard. The developed methodology can be applied to other datasets on a global or regional scale.

## 1 Introduction

Global flood hazard maps are an important tool in assessing global flood risk. They are used in reinsurance, large scale flood preparedness and emergency response and can also be used as benchmarks for future flood forecasting or climate impact assessment. It is often the case that flood hazard maps have been compiled at a national level or river catchment level. These smaller scale maps must then be aggregated to larger units, such as continents, in order to gain the large scale perspective (an example for such an initiative is EXCIMAP, 2007). In many countries across the globe such flood hazard maps are not available at the national level. In addition, the tiling





HESSD
9, 6615–6647, 2012



of maps generated by differing methods can create considerable inconsistencies, and the resulting uncertainties are not always clear from the finalised product. The use of large scale hydrological models and atmospheric land surface schemes for producing global scale hydrological products is of increasing interest (Cloke and Hannah, 2011) and have been employed on continental scale to derive flood hazard maps (Barredo et al., 2007). In this work we derive consistent global maps of flood return periods using a homogenous approach across the globe as a first step. The hazard maps could then be used in conjunction with vulnerability and impact information to produce global estimates of flood risk.

Global flood hazard maps are currently computed based on geomorphological regression, which uses non-linear regression of easily available geomorphological catchment attributes such as distance to river and upstream catchment area (Mehlhorn et al., 2005; SwissRe, 2012). Such methods have the considerable advantage of being able to calculate flood hazard zones to a very fine resolution using readily available data. An alternative method combines discharge observations with a simple river routing algorithm and flood outline observations (Herold et al., 2011). This method also uses regression to derive properties for ungauged catchments in which no observations exist. However, these methods make no use of available global scale information such as global time series of precipitation and they also lack application of hydrological understanding, including the hydrological processes operating in a river catchment, available spatial information and related physical understanding of land surface properties. They also make an implicit assumption that the method is transferable across a hydrologically and hydraulically diverse global land area. Such knowledge can however be included into a cascade of process based models, using meteorological models, hydrological models and hydraulic models. The concept of using a model cascade for global flood hazard prediction has been discussed by Winsemius et al. (2012). Physically based model cascades have been successfully employed in short-range, medium-range, monthly and seasonal forecasting of floods (Pappenberger et al., 2005, 2011; Alfieri et al., 2012; Voisin et al., 2011; Thielen et al., 2009) as well as projections of





HESSD
9, 6615–6647, 2012



climate impact on flooding (Cloke et al., 2010). Barredo et al. (2007) employed this technique successfully on a European continental level to derive flood hazard maps.

In this paper we derive a modelled global flood hazard map using the cascading models simulation approach with a number of products from the European Centre for Medium Range Weather Forecasts (ECMWF): ECMWF's land surface model, is forced with ERA-Interim reanalysis meteorological data (using a corrected precipitation) and the resulting runoff predictions are fed into a river routing algorithm which simulates floodplains and flood flow. The simulation period is 30 yr and a Gumbel distribution is fitted using annual maxima flows to derive a number of flood return periods. The latter is calculated on a 25 km × 25 km grid, which is then reprojected physically consistent with the routing model onto a 1 km × 1 km grid to derive maps of higher resolution and estimate flooded fractional area for the individual 25 km × 25 km cells. Thus the overall aim of this paper is to evaluate the derivation of globally consistent flood hazard maps to a resolution of 625 $km^2$ and 1 $km^2$ with ECMWF products. This is also a novel approach in evaluation and understanding of a coupled hydro-meteorological system on a global scale as previous studies have either focused on discharge (e.g. Pappenberger et al., 2010) or on observed flooded inundation fraction (e.g. Decharme et al., 2008, 2011; Dadson et al., 2010). This paper describes a proof-of-concept exercise and we carefully consider the limitations of this approach.

## 2 Method

In this study we derive global flood hazard maps using a cascading model simulation approach combined with ECMWF products and modelling systems. This cascade comprises four steps: (i) derivation of meteorological forcing data; (ii) physically based model chain; (iii) extreme value theory to derive return periods; (iv) remapping of results to required resolution. Each component of this cascade has been thoroughly tested with multiple calibration and validation studies.





HESSD
9, 6615–6647, 2012



## 2.1 Derivation of input data: ERA-Interim GPCP forcing

ERA-Interim (hereafter ERAI) is the latest global atmospheric reanalysis produced by ECMWF. ERAI covers the period from 1 January 1979 onwards, and continues to be extended forward in near-real time. Berrisford et al. (2009) provide a detailed description of the ERAI product archive. ERAI data, are freely available for access to researchers via ECMWF's webpage (http://www.ecmwf.int/research/era). Dee et al. (2011) present a detailed description of the ERAI model and data assimilation system, the observations used, and various performance aspects. Balsamo et al. (2011) preformed a scale-selective rescaling procedure to improve ERAI precipitation. The procedure corrects ERAI 3-hourly precipitation in order to match the monthly accumulation provided by the Global Precipitation Climatology Project (GPCP) v2.1 product (Huffman et al., 2009) at grid-point scale. The method uses information from GPCP v2.1 at the scale for which the dataset was provided (for a spatial resolution of $2.5^{\circ} \times 2.5^{\circ}$) and rescales the ERAI precipitation at full resolution (about $0.7^{\circ} \times 0.7^{\circ}$). The advantage of this procedure is that small scale features of ERAI (for instance related to orographic precipitation enhancement) can be preserved while the monthly totals are rescaled to match GPCP (see Balsamo et al., 2011; Szczypta et al., 2011).

## 2.2 Land surface model HTESSEL

In this study the Hydrology Tiled ECMWF Scheme of Surface Exchanges over Land (HTESSEL; Balsamo et al., 2009, 2011) is used. HTESSEL computes the land surface response to atmospheric forcing, and estimates the surface water and energy fluxes and the temporal evolution of soil temperature, moisture content and snowpack conditions. At the interface to the atmosphere each grid box is divided into fractions (tiles), with up to six fractions over land (bare ground, low and high vegetation, intercepted water, shaded and exposed snow). Vegetation types and cover fractions are derived from an external climate database, based on the Global Land Cover Characteristic (Loveland et al., 2000). The grid box surface fluxes are calculated separately for each tile,





HESSD
9, 6615–6647, 2012



leading to a separate solution of the surface energy balance equation and the skin temperature. The latter represents the interface between the soil and the atmosphere. The surface albedo is similar for all land tiles within a grid box except for those covered with snow. Below the surface, the vertical transfer of water and energy is performed using four vertical layers to represent soil temperature and moisture. Soil heat transfer follows a Fourier law of diffusion, modified to take into account soil water freezing/melting (Viterbo et al., 1999). Water movement in the soil is determined by Darcy's Law, and surface runoff accounts for the subgrid variability of orography (Balsamo et al., 2009). In the case of a partially (or fully) frozen soil, water transport is limited, leading to a redirection of most of the rainfall and snow melt to surface runoff when the uppermost soil layer is frozen. The snow scheme (Dutra et al., 2010) represents an additional layer on top of the soil, with an independent prognostic thermal and mass content. The snowpack is represented by a single snow temperature, snow mass, snow density, snow albedo, and a treatment for snow liquid water in the snowpack. Part of the liquid precipitation is directly intercepted by the canopy (that is evaporated at a potencial rate), and the remaining infiltrated in the soil, when snow is not present. When snow is present, liquid water is intercepted by the snowpack, and can freeze. Solid precipitation accumulates on the surface. The first soil layer receives liquid water from excess precipitation that was not intercepted in the canopy or snowpack, and also melted snow. Surface runoff is generated when the first soil layer is partially saturated. In the lowest model layer (2.89 m, constant globally) the boundary condition is free drainage, that produces the sub-surface runoff. Water is extracted from the soil via direct bare ground evaporation (only in the first soil layer), and by vegetation evapotranspiration (coupled to the surface energy balance).

HTESSEL is part of the integrated forecast system at ECMWF with operational applications ranging from the short-range to monthly and seasonal weather forecasts. HTESSEL is mainly used for operational forecasts coupled to the atmosphere, but it can also simulate the land surface evolution and exchanges with the atmosphere in stand-alone mode (commonly referred as "offline mode"). In offline mode, the model is





HESSD
9, 6615–6647, 2012



forced with sub-daily (at least 3-hourly) near surface meteorology (temperature, relative humidity, wind speed and surface pressure), and radiative (downward solar and thermal radiation) and water fluxes (liquid and solid precipitation). HTESSEL represents the land surface and soil vertical profile on a grid-point basis, with no horizontal exchanges. This offline methodology has been widely explored and calibrated in research applications using HTESSEL and other land surface and large scale hydrological models (e.g. Dutra et al., 2011; Haddeland et al., 2011), and also to derive land surface initial conditions of seasonal forecasts at ECMWF (Molteni et al., 2011).

### 2.3 River routing CaMa-flood

There are many different river routing algorithms which have been developed on a global scale (e.g. Miller et al., 1994; Arora and Boer, 1999; Ducharne et al., 2003) of which some include the explicit representation of flood plains and storage (Decharme et al., 2008, 2011; Dadson et al., 2008). The evaluation of these models either focuses on the impact of flood plains on discharge (e.g. Pappenberger et al., 2010) or compares modelled flooded inundation fraction with satellite observations (Decharme et al., 2008; Dadson et al., 2010). ECMWF has successfully employed several routing algorithms based on the TRIP model (Balsamo et al., 2011; Pappenberger et al., 2010). Yamazaki et al. (2011) developed this global routing methodology further by including flood plains into the routing algorithm through sub-grid parameterization of the floodplain topography. The sub-grid parameterization is based on a 1 km Digital Elevation Model and all horizontal water transport is modelled by a diffusive wave equation to account for backwater effects. Yamazaki et al. (2011) shows that this new model formulation (called CaMa-Flood) compares favourably to daily measurements of river flow gauging stations of all major rivers across the globe as well as indicating a good agreement between modelled and satellite observed flooded area. The river network construction, river parameters and sub-grid scale floodplain profiles are derived by the Flexible Location of Waterways (FLOW) method (Yamazaki et al., 2009). This method is used to upscale a high-resolution flow direction map into a coarse-resolution river





HESSD
9, 6615–6647, 2012



network map, which is used in by the global-scale river routing model. It also derives sub-grid-scale topographic parameters of the derived river network map (1 km × 1 km), such as channel length, channel altitude, unit-catchment area, and floodplain elevation profile. In the present configuration, the river network map was created at 25 km × 25 km resolution. This relationship is shown in Fig. 1. The outlet on the regular 25 km × 25 km grid is indicated by a circle. The routing characteristics are based on the upstream catchment which may span several 25 km × 25 km cells. One of the characteristics is elevation profile which is shown in the bottom subfigure of Fig. 1, where the topographic height is plotted against the fraction which would be flooded at this height. The daily HTESSEL simulated surface and sub-surface runoff, at 80 km × 80 km resolution, is interpolated to the river network resolution using a nearest neighbour approach.

### 2.4 Extreme value theory to estimating return periods

The return period estimation is based on the annual maxima of the river storage produced by CaMa-Flood. There are many different statistical distributions which can be used in the estimation of flood frequency, ranging from general logistics distributions in countries such as the UK (Reed et al., 2010) to the log Pearson Type III in the USA (IACWD, 1982). In this study, the aim was to apply the same modelling method across the globe constrained by data availability (e.g. time series of only 30 yr available from ERA-Interim) and computational resources (e.g. requirement for dynamic distribution fitting in every cell across the global land area). Therefore the Gumbel distribution (EV1) estimated using L-moments was chosen whose two parameters can be easily estimated by the method of moments and which allows the cheap computation of confidence limits for the fitted data. The method is described in detail in Shaw et al. (2011). The EV1 distribution was computed for the river storage annual maxima on the 25 km grid and 2, 5, 10, 20, 50, 75, 100, 200, 500 yr return periods calculated. The respective river storages were converted to water levels using the river network parameters, river length and width. The water levels could then be used to establish whether the river has gone out of bank and whether cells are flooded or not flooded.





HESSD
9, 6615–6647, 2012



## 2.5 Remapping of required resolution

CaMa-Flood produces river storage on a 25 km × 25 km grid. This river storage is representative of the sub-catchment, whose sub-grid parameters (floodplain profile, Yamazaki et al., 2009), were considered during the simulations. These sub-grib parameters are derived from the 1 km × 1 km cells. Therefore, the river water level (derived from river storage – using river length and width) can be remapped into the 1 km × 1 km grid consistently with the model structure and assumptions. The river water level in each 25 km × 25 km grid, is remapped to the 1 km × 1 km grid allowing the identification of flooded and not-flooded pixels (as displayed in Fig. 1). The approach in this paper is equivalent to a volume filling approach as shown by Winsemius (2012) with the additional advantage that the subgrid parameterization actually influences the river routing . This information is then upscaled to the 25 km × 25 km grid to derive fractional coverage by re-aggregating all respective 1 km × 1 km cells.

## 2.6 Evaluation of hazard maps

### 2.6.1 Benchmark data set

A global flood hazard map has been produced for the 2011 Global Assessment Report on Disaster Risk Reduction (Herold et al., 2011; Herold and Mouton, 2011). In this report, peak flow values for 100 yr return periods have been estimated for gauged sites and regionalized by clustering observations from river gauging stations and using regression to estimate return periods for ungauged sites. Peak flow values have been routed through the catchments to derive flooded area. These data have then been merged with data from actual flood events observed by the Dartmouth Flood Observatory (www.dartmouth.edu/~floods/) to derive maps indicating different return periods. A description of the procedure is given in Herold and Mouton (2011) where also some verification for individual catchments is shown. All data can be downloaded from the Global Risk Data platform (http://preview.grid.unep.ch/). Please note that we do not





HESSD
9, 6615–6647, 2012



assume "correctness" of the data set and rather use this data set as a benchmark to establish whether the methodology used in this paper leads to similar results.

### 2.6.2 Benchmark comparison score

In this study the global flood hazard results are compared to the benchmark data set using three scores which are designed to evaluate extremes: the Equitable Threat Score (ETS, Hogan et al., 2010; Doswell et al., 1990; Gandin and Murphy, 1992), the Extreme Dependency Score (EDS, Stephenson, 2008) and the Frequency Bias (FB; Gandin and Murphy, 1992):

The ETS is based on a contingency table (see Table 1) and compares the hits and correct negatives events of the benchmark data set to the hits + correct negatives events of the data set created in this study. The score ranges from $-1/3$ to 1 (perfect score) with 0 indicating that there is no skill (skill indicated by random chance). The score takes account of false alarms and missed events.

The EDS evaluates the association between forecasted and observed rare events based on hits and misses (not explicitly evaluating false alarms). It ranges from $-1$ to 1 (perfect score) with 0 indicating that there is no skill. The EDS is not sensitive to bias and thus needs to be complemented by the frequency bias.

The FB measures whether the frequency of the two data set is similar. A FB $> 1$ indicates that there is a positive bias (over forecasting) of the data set computed in this study in comparison to the benchmark data set (and vice versa). It ranges from 0 to $\infty$, with 1 indicating a perfect score.

## 3 Results

### 3.1 The global flood return period maps

Figure 2 shows the major river basins of the world to aid interpretation and discussion of the results. The total area of floodplains given by a 1000 year return period is calculated





HESSD
9, 6615–6647, 2012



as $1.9 \times 10^6$ km$^2$ which is within the limits of other global estimates ranging from 0.8–2 × $10^6$ km$^2$ (Mitsch and Gosselink, 2000; Ramsar and IUCN (World Conservation Union), 1999). In Fig. 3, the areal fraction of coverage of flooding occurring in the 25 km by 25 km cells is shown for a 50 yr return period. 1 means that the cell is completely flooded across its area, 0.5 means that 50 % of the area within the cell is flooded and 0 means that the area is not flooded at all. A minimum threshold of 5 % has been set for display purposes. As would be expected, flood hazard at a 50 yr return period shows up as a wide-spread phenomenon occurring at many locations on the globe and many major catchments can be clearly seen in Fig. 2. In addition some lakes such as the Great lakes in Northern America, which are not explicitly modelled within the routing component, show as 100 % flooded. There are also delta areas which can be clearly seen, for example the Mississippi in North America, the Yangtze and Hunag He in China, the Indus on the Indian sub continent as well as the Ganges and Brahmaputra, the Euphrates and Tigris and the Murray Darling in Australia. In Africa the upper Niger catchment, the Lake Chad catchment as well as the Congo show not only in the in the delta area, but particularly in land. In South America, the Amazon and Parana catchments are dominant. Many other areas with high fractional coverage can be seen in Asia (e.g. Volga into the Black Sea or the Kolyma).

Figure 4 shows how flood hazard increases with return period for the 20 largest catchments calculated as the average area of floodplains flooded (maximum extent of floodplains are estimated from computing a 1000 yr return period). The figure shows an average flooding of around 45 % of all floodplains within all major catchments to over 90 % at higher return periods. This information could be used in the calculation of the number of people or properties are affected by a flood event of a certain return period and analysis of this on a global or continental scale (see e.g. Winsemius et al., 2012).

It is of particular interest in many applications to analyse these maps at the continental scale. Figure 5a displays the fractional coverage on a 25 km$^2$ grid for a 50 yr return period for Europe. To aid in the interpretation of the results some of the major rivers of Europe are overlaid as blue lines. The flooded area follows those lines fairly closely





HESSD
9, 6615–6647, 2012



(see for example the rivers Po and Danube), indicating that the resulting maps have some credibility. Even smaller rivers which are not explicitly plotted as major rivers can be seen (e.g. the Tisza). The effect of lakes can also be seen as was the case for the global results. These maps are derived from 1 km$^2$ re-projections, which is shown as an example in Fig. 5b. The similarities between Fig. 5a, b are encouraging, although Fig. 5b clearly shows more detail. It would be possible in theory to interpolate to even finer topographic resolutions (e.g. 90 m of the SRTM data set as in Herold and Mouton, 2011), however, given the coarse resolution and uncertainties in the many other data inputs, this course of action is not recommended as the uncertainties would be very high, even though a higher resolution image would of course look more attractive (see discussion on hyperresolved modelling in Beven and Cloke, 2012). In all modelling exercises an appreciation of the uncertainties involved is paramount (Pappenberger and Beven, 2006). We demonstrate this uncertainty in Table 2 and Fig. 4.

Figure 5c shows the 50 yr return period map for South America focusing on the Amazon catchment in particular. As for Fig. 5a, the major rivers are followed, but here the complexity of the channel network in the Amazon basin can be clearly seen. Which is encouraging as such complexity demonstrates the value of subgrid representation of the channel network. Note, the major lakes such as the Titicaca and Poopo are also picked up in the flooded pixels.

Table 2 shows the average percentage of floodplain flooded in 25 km$^2$ grid cells for individual river catchments. It is obvious that the fraction increases with increasing return period as seen in Fig. 4. One should take particular notice of the uncertainty bounds around the median. These uncertainty bounds increase with increasing return period, however, they are not very large. This maybe be explained by the fact that a large uncertainty in discharge does not translate to an equally large uncertainty in extent because of the valley filling phenomenon of floods over a certain magnitude (Schumann et al., 2009; Pappenberger et al., 2006). Uncertainty in the estimation of the return period has to be large enough to cover individual 1 km cells, which may





HESSD
9, 6615–6647, 2012



require significant jumps in water level. These findings are also illustrated when the average over all 20 catchments is displayed (Fig. 4).

### 3.2 Comparison with benchmark data set

The benchmark data set is shown in Fig. 6a, b for a 50 yr return period, which are equivalent to the representations of the model cascade flood hazard depicted in Fig. 5a, b. A comparison of Figs. 6a and 5a shows that the benchmark data set displays greater detail but has a lower intensity of flooding depicted for a 50 yr return period. Figure 6b shows a far more detailed river network than Fig. 5b because it has been computed by a river routing algorithm on a finer scale (90 m SRTM data). However it also indicates a much lower extent of individual floodplains, which suggests that the 50 yr return period river discharges are calculated to be greater in this study then this in the benchmark. This is probably a result of the longer time series in this study or alternatively maybe reasoned in different representations of floodplain and channel storage.

Major rivers are equally well represented in the benchmark data set as in the data set of this study. Figure 7 directly compares the global flood hazard results with the benchmark set for major catchments. It is encouraging to observe some clear correlation between the modelled and observed data, as they have been derived by considerably different methodologies. This correlation is shown by the high number of hits and correct negatives, which always exceed false alarms and misses. It is important to note that neither data set represents the truth and this exercise seeks to compare in order to identify differences and allow the exploration of the properties of the data set produced in this study. There are also more hits than false alarms, but more false alarms than misses at higher return periods, which suggests that the methodology in this paper produces larger areas of flooding than the benchmark data set.

The values of the contingency table (hits, misses and false alarms) shown in Fig. 7 can be used to calculate an agreement between the two data sets using scores such as the Equitable Threat Score (ETS). The ETS is displayed in Fig. 8 as an average over the largest 20 catchments. The ETS reaches an optimal score at 1 and is skillfull in





HESSD
9, 6615–6647, 2012



comparison to a random guess for values above 0. It is reassuring to observe that the ETS is above 0 for all return periods although the flattening of the curve at higher return periods indicate that a random benchmark is not too difficult to beat in this case. The ETS peaks at a return period of 20 yr indicating that the maps are in closest agreement at this return period. The Extreme Dependency Score does not illustrate this peak. This is explained by the fact that it does not explicitly incorporate false alarms which increase with increasing return period. It is influenced from a continuous increase in hits and decrease in misses. The score is always above 0 indicating skill at all return periods. This skill maybe purely topographically driven. The frequency bias is below 1 for the 2 and 5 yr return period and above one for higher return periods. This indicates that the benchmark has a higher number of flooded cells for a return period of 2 and 5 and a lower number of flooded cells than this study's results for larger return periods in comparison to the data set computed in this study.

## 4 Discussion

### 4.1 What did we learn?

This proof-of-concept study has demonstrated the potential for using the products of a modern Numerical Weather Prediction Centre to produce relevant global information on flood hazard. Using a relatively simple but globally consistent methodology produced an encouraging global hazard data set with information on return periods at 25 and 1 km scale. All tools and products are available for free for research purposes and can be downloaded from various sources on the internet. The global flood hazard maps derived by different methods produce broadly similar results. The uncertainty in the estimation of flood extent is not dominated by the uncertainty in the estimation of the extreme value distribution deployed but instead it is likely dependent on the parameter uncertainty and model processes. Further definition of the characteristic uncertainties of the maps will be required.





HESSD
9, 6615–6647, 2012



### 4.2 How useful are the results?

A global picture of flood hazard will be very useful for current and future understanding of flood risk. However, this can only be supported by a thorough understanding of the limitations involved. This study ignores many important components such as operating rules of dams and reservoirs, protection structures and so forth. Although reasonably complicated to undertake at a global scale, such effects could be included by sub-grid parameterization. Herold et al. (2011) demonstrates the point with the example of the Bihar floods in 2008 in which a dyke breach causes significant difference between the modelled and observed flood outlines. Herold et al. (2011) carries the clear warning that global models should not be used for local planning. However, although results may be wrong on a local scale, they can have a useful credibility on a global scale for large scale assessment. This usefulness and credibility comes through the averaging or coarse graining which is achieved in this study. One should not analyse the behaviour of individual cells but of a (catchment) group of cells. This will then enable going beyond the quantification of hazard, to the derivation of risk and impact maps. Such maps could be used for insurance purposes or the direction of global investment, for example deriving priority regions in which an upgrading of river defence structures may result in the highest return in terms of impact. This information on its own has limited value, although it is essential for combination with other information to produce increased value as one could for example not compute hazard without flood frequency. These global maps have an additional advantage of allowing for the provision of initial information about unknown areas.

One of the main motivations in the application of the global framework was to achieve globally consistent maps, meaning that a grid point value in Honduras has been derived in the same way as one in Nepal. This is of course only partially true as for example the quality and behaviour underlying meteorological forcing is dependent on the local geography (a similar argument can be made for the hydrology). However, this approach





HESSD
9, 6615–6647, 2012



still provides a homogeneous framework allowing for the flexibility to improve locally where necessary and when.

### 4.3 Future improvements

This is a proof of concept study, which seeks to calculate global flood hazard maps with a coherent methodology using global scale models and datasets. Future work will focus on improving the individual components of the model cascade.

In stage I (derivation of forcing data), the data set used in this study may be substantially improved upo by using an enhanced correction routine or better correction data (see e.g. Weedon et al., 2012). The ERAInterim reanalysis is too short and would be better replaced by a longer reanalysis data set, such as the forthcoming ERA-CLIM, (www.era-clim.eu/). A longer time series would be able to catch more extreme events and hence allow for an improved estimation of extremes. The use of stochastic weather generators and downscaling could also improve the quality of the input data set.

There are many aspects of the land surface scheme of stage II (physically based models) that could be improved (e.g. representation of ground water table see ECMWF, 2010 or consideration of hydrological parameter uncertainty, Cloke et al., 2011). This is valid for the land surface component as well as the river routing model which may benefit from additional calibration, regionalisation and inclusion of sub-grid representations. Alternative physical and non-physical hydrological schemes could be considered. The physical model cascade has another additional clear disadvantage as it includes a larger number of parameters in comparison to the simpler geomorphological regression. Such complexity leads to considerable uncertainties and equifinalities in the model parameters and structure (Beven and Binley, 1992). In this study we solely estimated uncertainties stemming from the fitting of the extreme value distribution which will clearly underestimate the total uncertainty. Future studies have to take greater care in the quantification of this uncertainty, which maybe difficult given the large number of models and processes involved.





HESSD
9, 6615–6647, 2012



In this study one simple extreme value distribution was assumed for stage III (extreme value theory to derive return periods). Hydrological understanding of flood generating processes suggests that mixed distributions should be used (Woo and Waylen, 1984; Merz and Bloschl, 2005). Future developments may need to apply a host of different distributions. An alternative method may be possible through extending the data set as mentioned above for stage I. Such an extension could eventually could allow estimation of return periods using continuous simulations (see e.g. Blazkova and Beven, 2002). This would allow stage III (extreme value theory to derive return periods) to be omitted from this estimation cascade and reduce a major source of uncertainty.

Re-mapping of stage IV to the required resolution is in this study done by interpolating respecting a particular subgrid parameterisation. Re-mapping requires careful balancing of what is possible (e.g. a 90 m resolved flood hazard map) with what is scientifically justifiable accepting that resolution alone does not increase the information content (Beven and Cloke, 2011). Future studies should attempt to push the resolution boundary whilst not pretending to be able to do the impossible.

Comparison has been performed against a single global benchmark data set and further comparison is ideally required. Future analysis should use local data for comparison and employ further scores. In addition, the physical processes that determine the dynamics of flood inundation behaviour should be included in future versions.

Many of the improvements discussed above are areas of active research, which also illustrates the strength of this methodology. Most of the individual components are active parts of operational forecasting chains with clear commitments by individual organisations (such as ECMWF) to improve them. This means that there is a continuous development on the individual components of this system.

## 5 Conclusions

The aim of this paper is to demonstrate a methodology to derive global flood hazard maps which are derived by a consistent approach across the globe. This study is





HESSD
9, 6615–6647, 2012



based on products of the European Centre For Medium range Weather Forecasts and uses models and data which are freely available. The application of a methodology on a global scale naturally includes many assumptions and therefore this study has to be seen as a proof of concept.

In this paper the flood hazard maps for different return periods are derived from a cascade of models and data. The major source of the atmospheric forcing is derived form reanalysis data (ERAInterim) corrected with observations (GPCP data). These inputs are used to as boundary conditions to the an operational land surface scheme named HTessel whose results in turn are fed into a river routing algorithm which simulates and represented floodplains (CaMa-Flood). A map of global river discharge on a 25 km scale is produced (the 25 km contains subgrid parameterization from a 1 km resolved grid). Return periods up to 1000 yr are computed by fitting a Gumble distribution to the river discharge. River discharge is converted into river level through a rating curve and flooding is remapped onto a 1 $km^2$ grid. We demonstrate that the resulting maps are physically plausible by showing the analyses of global and continental maps of the 50 yr return period. Uncertainty in this study is estimated from the fitting of the distribution and is relatively low to what one would expect. This is explained by the fact that uncertainty in discharge is somewhat dampened if mapped into a flood inundation. This study also compares the results to a benchmark produced by the Herold and Mouton (2011) using a different methodology. In general the benchmark has a higher number of flooded cells for a return period of 2 and 5 and a lower number of flooded cells for larger return periods (>20 yr) in comparison to the data set computed in this study.

The results of this study indicate that the approach in this paper is feasible and can produce realistic global flood hazard maps of various return periods. It can be used to either gain a global overview and prompt further research on the local scale. Limitations can be overcome by addressing each component of the system individually. The approach has the great advantage that it benefits from continuous model developments and improvements as most components are part of an operational forecast chain.





HESSD
9, 6615–6647, 2012



*Acknowledgements.* This work was funded by the KultuRisk (Fp7, http://www.kulturisk.eu/) and DEMON (NERC Storm Risk Mitigation Programme Project, NE/I005242/1) project.

## References

Alfieri, L., Salamon, P., Pappenberger, F., Wetterhall, F., and Thielen, J.: Operational early warning systems for water-related hazards in Europe, 2012, Environ. Sci. Policy, 21, 35–49, doi:10.1016/j.envsci.2012.01.008, 2012.

Arora, V. K. and Boer, G. J.: A variable velocity flow routing algorithm for GCMs, J. Geophys. Res., 104, 30965–30979, 1999.

Balsamo, G., Viterbo, P., Beljaars, A., Van den Hurk, B., Betts, A. K., and Scipal, K.: A revised hydrology for the ECMWF model: verification from field site to terrestrial water storage and impact in the Integrated Forecast System, J. Hydrometeorol., 10, 623–643 doi:10.1175/2008JHM1068.1171, 2009.

Balsamo, G., Pappenberger, F., Dutra, E., Viterbo, P., and van den Hurk, B.: A revised land hydrology in the ECMWF model: a step towards daily water flux prediction in a fully-closed water cycle, Hydrol. Process., 25, 1046–1054, doi:10.1002/hyp.7808, 2011.

Barredo, J. I., de Roo, A., and Lavalle, C.: Flood risk mapping at European scale, Water Sci. Technol., 56, 11–17, 2007.

Beven, K. J. and H. L. Cloke: Comment on "Hyperresolution global land surface modeling: Meeting a grand challenge for monitoring Earth's terrestrial water" by Eric F. Wood et al., Water Resour. Res., 48, W01801, doi:10.1029/2011WR010982, 2012.

Blazkova, S. and Beven, K. J.: Flood frequency estimation by continuous simulation for a catchment treated as ungauged (with uncertainty), Water Resour. Res., 38, 1139, doi:10.1029/2001WR000500, 2002.

Cloke, H. L. and Hannah, D. M.: Large-scale hydrology: advances in understanding processes, dynamics and models from beyond river basin to global scale, Hydrol. Process., 25, 991–995, doi:10.1002/hyp.8059, 2011.

Cloke, H. L., Jeffers, C., Wetterhall, F., Byrne, T., Lowe J., and Pappenberger, F.: Climate impacts on river flow: projections for the Medway catchment, UK, with UKCP09 and CATCHMOD, Hydrol. Process., 24, 3476–3489, doi:10.1002/hyp.7769, 2010.





HESSD

9, 6615–6647, 2012



Cloke, H. L., Weisheimer, A., and Pappenberger, F.: Representing uncertainty in land surface hydrology: fully coupled simulations with the ECMWF land surface scheme, in: Proceedings of the ECMWF/WMO/WCRP workshop on "Representing Model Uncertainty and Error in Numerical Weather and Climate Prediction Models", 20–24 June 2011 at ECMWF, Reading, UK, 2011.

Dadson, S. J., Ashpole, I., Harris, P., Davies, H. N., Clark, D. B., Blyth, E., and Taylor, C. M.: Wetland inundation dynamics in a model of land surface climate: evaluation in the Niger inland delta region, J. Geophys. Res., 115, D23114, doi:10.1029/2010JD014474, 2010.

Decharme, B., Douville, H., Prigent, C., Papa, F., and Aires, F.: A new river flooding scheme for global climate applications: off-line evaluation over South America, J. Geophys. Res., 113, D11110, doi:10.1029/2007JD009376, 2008.

Decharme, B., Alkama, R., Douville, H., Prigent, C., Papa, F., and Faroux, S.: Global off-line evaluation of the ISBA-TRIP flood model, Clim. Dynam., 38, 1389–1412, doi:10.1007/s00382-011-1054-9, 2011.

Doswell, C. A., Davies-Jones III, R., and Keller, D. L.: On summary measures of skill in rare event forecasting based on contingency tables, Weather Forecast., 5, 576–586, 1990.

Dutra, E., Balsamo, G., Viterbo, P., Miranda, P. M. A., Beljaars, A., Schar, C., and Elder, K.: An improved snow scheme for the ECMWF land surface model: description and offline validation, J. Hydrometeorol., 11, 899–916, doi:10.1175/2010jhm1249.1, 2010.

Dutra, E., Kotlarski, S., Viterbo, P., Balsamo, G., Miranda, P. M. A., Schär, C., Bissolli, P., and Jonas, T.: Snow cover sensitivity to horizontal resolution, parameterizations, and atmospheric forcing in a land surface model, J. Geophys. Res., 116, D21109, doi:10.1029/2011jd016061, 2011.

Ducharne, A., Golaz, C., Leblois, E., Laval, K., Polcher, J., Ledoux, E., and de Marsily, G.: Development of a high resolution runoff routing model, calibration and application to assess runoff from the LMD GCM, J. Hydrol., 280, 207–228, doi:10.1016/S0022-1694(03)00230-0, 2003.

ECMWF: The ECMWF Strategy 2011–2020, available at: http://www.ecmwf.int/about/programmatic/strategy/Strategy-2011-20-v2.6-1.pdf (last access: 24 May 2012), 2010.

EXCIMAP (European Exchange Circle on Flood Mapping): Handbook of good practices in flood mapping and an atlas of flood maps, available at: http://floods.jrc.ec.europa.eu/flood-risk/excimap-handbook-on-flood-mapping (last access: 13 April 2012), 2007.





HESSD
9, 6615–6647, 2012



Gandin, K. S. and Murphy, A. H.: Equitable scores for categorical forecasts, Mon. Weather Rev., 120, 361–370, 1992.
Haddeland, I., Clark, D., Franssen, W. H. P., Ludwig, F., Voss, F., Arnell, N. W., Bertrand, N., Best, M., Folwell, S., Gerten, D., Gomes, S., Gosling, S., Hagemann, S., Hanasaki, N., Harding, R., Heinke, J., Kabat, P., Koirala, S., Oki, T., Polcher, J., Stacke, T., Viterbo, P., Weedon, G. P., and Yeh, P.: Multimodel estimate of the global terrestrial water balance: setup and first results, J. Hydrometeorol., 12, 869–884, doi:10.1175/2011jhm1324.1, 2011.
Herold, C. and Mouton, F.: Global flood hazard mapping using statistical peak flow estimates, Hydrol. Earth Syst. Sci. Discuss., 8, 305–363, doi:10.5194/hessd-8-305-2011, 2011.
Herold, C., Mouton, F., Verdin, K., Verdin, J., Brackenridge, R., Liu, Z., Tyagi, A., and Grabs, W.: Floods, Appendix 1: Global Risk Analysis, Global Assessment Report 2009, available online: http://www.preventionweb.net/english/hyogo/gar/appendices/documents/Appendix-1.doc (last access: 11 April 2012), 2011.
Hogan, R. J., Ferro, C. A. T., Jolliffe, I. T., and Stephenson, D. B.: Equitability revisited: why the "Equitable Threat Score" is not equitable, Weather Forecast., 25, 710–726, doi:10.1175/2009WAF2222350.1, 2010.
IACWD (Interagency Advisory Committee on Water Data): Guidelines for determining flood-flow frequency: Bulletin 17B, Hydrology Subcommittee, Office of Water Data Coordination, US Geological Survey, Reston, Va., 183 pp., available at: http://water.usgs.gov/osw/bulletin17b/bulletin_17B.html (last access: 24 May 2012), 1982.
Mehlhorn, J., Feyen, F., Banovsky, I., and Menzinger, I.: FRAT1.0 – an example of applying the geomorphologic regression approach for detailed single location flood risk assessment, Geophys. Res. Abstr., 7, 07419, available at: http://meetings.copernicus.org/www.cosis.net/abstracts/EGU05/07419/EGU05-J-07419.pdf (last access: 25 May 2012), 2005.
Merz, R. and Bloeschl, G.: Flood frequency regionalisation – spatial proximity vs. catchment attributes, J. Hydrol., 302, 283–306, 2005.
Miller, J. R., Russell, G. L., and Caliri, G.: Continental-scale river flow in climate models, J. Climate, 7, 914–928, doi:10.1175/1520-0442(1994)007<0914:CSRFIC>2.0.CO;2, 1994.
Mitsch, W. J. and Gosselink, J. G.: Wetlands, Wiley, New York, USA, 2000.
Molteni, F., Stockdale, T., Balmaseda, M., Balsamo, G., Buizza, R., Ferranti, L., Magnusson, L., Mogensen, K., Palmer, T., and Vitart, F.: The new ECMWF seasonal forecast system (System 4), ECMWF Tech memo, 656, 49 pp., issued by ECMWF, Reading, UK, avail-





HESSD
9, 6615–6647, 2012



able at: http://www.ecmwf.int/publications/library/do/references/show?id=90277 (last access: 24 May 2012), 2011.
Pappenberger, F. and Beven, K. J.: Ignorance is bliss – or 7 reasons not to use uncertainty analysis, Water Resour. Res., 42, W05302, doi:10.1029/2005WR004820, 2006.
Pappenberger, F., Matgen, P., Beven, K. J., Henry, J. B., Pfister, L., and de Fraipont, P.: Influence of uncertain boundary conditions and model structure on flood inundation predictions, Adv. Water Resour., 29, 1430–1449, 2006.
Pappenberger, F., Cloke, H. L., Balsamo, G., Oki, P., and Ngo-Duc, T.: Global routing of surface and subsurface runoff produced by the hydrological component of the ECMWF NWP system, Int. J. Climatol., 30, 2155–2174, 2010.
Pappenberger, F., Thielen, J., and Del Medico, M.: The impact of weather forecast improvements on large scale hydrology: analysing a decade of forecasts of the European Flood Alert System, Hydrol. Process., 25, 1091–1113, doi:10.1002/hyp.7772, 2011.
Ramsar and IUCN: Wetlands and global change, available at: http://www.ramsar.org/cda/en/ramsar-documents-wetlands-and-climate/main/ramsar/1-31%5E21076_4000_0 (last access: 24 May 2012), 1999.
Reed, D. W., Faulkner, D., Robson, A., Houghton-Carr, H., and Bayliss, A. C.: Flood Estimation Handbook, Centre for Ecology & Hydrology, Wallingford, UK, 2002.
Schumann, G., Bates, P. D., Horritt, M. S., Matgen, P., and Pappenberger, F.: Progress in integration of remote sensing-derived flood extent and stage data and hydraulic models, Rev. Geophys., 47, RG4001, doi:10.1029/2008RG000274, 2009.
Shaw, E. M., Beven, K. J., Chappell, N. A., and Lamb, R.: Hydrology in Practice, 4th Edn., Taylor and Francis, Abingdon, Spon Press, London, 2011.
Stephenson, D. B., Casati, B., Ferro, C. A. T., and Wilson, C. A.: The extreme dependency score: a non-vanishing measure for forecasts of rare events, Meteorol. Appl., 15, 41–50, 2008.
SwissRe, available at: http://www.swissre.com/clients/insurers/property_casualty/Swiss_Re_Global_Flood_Zones_enabling_better_business_decisions.html, last access: 16 April, 2012.
Thielen, J., Bogner, K., Pappenberger, F., Kalas, M., del Medico, M., and de Roo, A.: Monthly-, medium- and short range flood warning: testing the limits of predictability, Meteorol. Appl., 16, 77–90, 2009.





HESSD
9, 6615–6647, 2012



Voisin, N., Pappenberger, F., Lettenmaier, D. P., Buizza, R., and Schaake, J. C.: Application of a medium-range global hydrologic probabilistic forecast scheme to the Ohio River basin, Weather Forecast., 26, 425–446, 2011.

Weedon, G. P., Gomes, S., Viterbo, P., Shuttleworth, W. J., Blyth, E., Österle, H., Adam, H., Bellouin, N., Boucher, O., and Best, M.: Creation of the WATCH Forcing Data and its use to assess global and regional reference crop evaporation over land during the twentieth century, J. Hydrometeorol., 12, 823–848, 2012.

Woo, M. K. and Waylen, P.: Areal prediction of annual floods generated by two distinct processes, Hydrol. Sci. J., 29, 75–88, 1984.

Yamazaki, D., Oki, T., and Kanae, S.: Deriving a global river network map and its sub-grid topographic characteristics from a fine-resolution flow direction map, Hydrol. Earth Syst. Sci., 13, 2241–2251, doi:10.5194/hess-13-2241-2009, 2009.

Yamazaki, D., Kanae, S., Kim, H., and Oki, T.: A physically based description of floodplain inundation dynamics in a global river routing model, Water Resour. Res., 47, W04501, doi:10.1029/2010WR009726, 2011.

Winsemius, H. C., van Beek, L., Bouwman, A., Ward, P. J., and Jongman, B.: A framework for global river flood risk assessments, EGU 2012, available at: http://meetingorganizer.copernicus.org/EGU2012/EGU2012-6237.pdf (last access: 24 May 2012), 2012.





HESSD

9, 6615–6647, 2012



**Table 1.** Contingency table.

| | | Benchmark data set | |
|---|---|---|---|
| | | Yes | No |
| Data set produced in this study | Yes | Hit | False Alarm |
| | No | Miss | Correct Negative |





HESSD
9, 6615–6647, 2012



**Table 2.** Percentage of floodplain flooded in 20 major catchments (25 km global grid) and multiple return periods. The table shows the median and the 5th and 95th percentile.

| Id | Catchment | Return Period | | | | | | | | |
|---|---|---|---|---|---|---|---|---|---|---|
| (Fig. 2) | | 2 | 5 | 10 | 20 | 50 | 75 | 100 | 200 | 500 |
| 1 | Yukon | 57.78 ± 0.02 | 66.53 ± 0.09 | 71.49 ± 0.05 | 76.38 ± 0.19 | 83.00 ± 0.05 | 85.24 ± 0.12 | 87.01 ± 0.09 | 91.27 ± 0.17 | 96.88 ± 0.23 |
| 2 | Mackenzie | 53.36 ± 0.01 | 61.91 ± 0.09 | 67.55 ± 0.11 | 72.88 ± 0.06 | 79.61 ± 0.16 | 82.41 ± 0.18 | 84.31 ± 0.17 | 88.98 ± 0.21 | 95.52 ± 0.20 |
| 3 | Nelson | 37.23 ± 0.01 | 47.60 ± 0.15 | 54.57 ± 0.10 | 60.46 ± 0.11 | 69.03 ± 0.25 | 72.62 ± 0.31 | 75.72 ± 0.26 | 82.85 ± 0.39 | 92.67 ± 0.48 |
| 4 | Mississippi | 33.82 ± 0.04 | 44.74 ± 0.12 | 52.37 ± 0.12 | 59.15 ± 0.18 | 68.54 ± 0.31 | 72.61 ± 0.25 | 75.75 ± 0.28 | 82.99 ± 0.33 | 92.81 ± 0.45 |
| 5 | St Lawrence | 56.69 ± 0.03 | 64.28 ± 0.08 | 69.46 ± 0.13 | 74.08 ± 0.05 | 79.81 ± 0.15 | 82.28 ± 0.17 | 84.39 ± 0.29 | 88.98 ± 0.11 | 95.35 ± 0.15 |
| 6 | Amazon | 40.74 ± 0.07 | 49.60 ± 0.09 | 55.56 ± 0.13 | 61.64 ± 0.15 | 69.97 ± 0.21 | 73.61 ± 0.23 | 76.29 ± 0.23 | 82.99 ± 0.30 | 92.43 ± 0.41 |
| 7 | Parana | 33.21 ± 0.04 | 43.61 ± 0.11 | 50.69 ± 0.09 | 57.70 ± 0.17 | 66.99 ± 0.24 | 71.15 ± 0.23 | 74.34 ± 0.30 | 81.83 ± 0.28 | 92.17 ± 0.41 |
| 8 | Niger | 28.27 ± 0.02 | 35.85 ± 0.08 | 42.60 ± 0.07 | 49.68 ± 0.22 | 60.12 ± 0.28 | 65.26 ± 0.32 | 68.83 ± 0.28 | 77.79 ± 0.37 | 90.49 ± 0.51 |
| 10 | Congo | 36.05 ± 0.06 | 45.80 ± 0.07 | 52.11 ± 0.14 | 58.78 ± 0.18 | 67.73 ± 0.25 | 71.64 ± 0.22 | 74.61 ± 0.29 | 82.04 ± 0.38 | 92.09 ± 0.41 |
| 11 | Nile | 49.28 ± 0.02 | 56.05 ± 0.04 | 60.97 ± 0.07 | 66.48 ± 0.15 | 73.80 ± 0.18 | 77.12 ± 0.22 | 79.38 ± 0.23 | 85.40 ± 0.24 | 93.75 ± 0.35 |
| 12 | Zambezi | 28.58 ± 0.05 | 41.22 ± 0.09 | 49.16 ± 0.21 | 56.20 ± 0.18 | 65.81 ± 0.30 | 70.38 ± 0.28 | 73.81 ± 0.29 | 81.16 ± 0.40 | 91.32 ± 0.33 |
| 13 | Volga | 39.22 ± 0.05 | 49.79 ± 0.10 | 56.64 ± 0.11 | 63.39 ± 0.17 | 71.78 ± 0.14 | 75.12 ± 0.21 | 77.94 ± 0.27 | 84.49 ± 0.29 | 93.24 ± 0.39 |
| 14 | Ob | 43.03 ± 0.06 | 51.99 ± 0.06 | 58.31 ± 0.15 | 64.23 ± 0.17 | 72.41 ± 0.25 | 76.06 ± 0.23 | 78.69 ± 0.20 | 85.05 ± 0.27 | 93.45 ± 0.33 |
| 15 | Yenisey | 55.40 ± 0.04 | 64.21 ± 0.03 | 69.82 ± 0.09 | 74.78 ± 0.08 | 80.96 ± 0.12 | 83.64 ± 0.23 | 85.42 ± 0.14 | 90.01 ± 0.16 | 95.82 ± 0.20 |
| 16 | Lena | 52.73 ± 0.03 | 62.88 ± 0.12 | 68.72 ± 0.09 | 73.81 ± 0.11 | 80.29 ± 0.19 | 83.06 ± 0.15 | 85.08 ± 0.17 | 89.91 ± 0.28 | 95.63 ± 0.23 |
| 17 | Kolyma | 60.11 ± 0.03 | 68.40 ± 0.12 | 73.88 ± 0.12 | 78.48 ± 0.12 | 84.30 ± 0.06 | 86.51 ± 0.10 | 88.14 ± 0.15 | 92.02 ± 0.09 | 96.78 ± 0.24 |
| 18 | Amur | 40.87 ± 0.12 | 52.58 ± 0.14 | 59.72 ± 0.12 | 66.18 ± 0.20 | 74.30 ± 0.23 | 78.03 ± 0.28 | 80.52 ± 0.30 | 86.52 ± 0.34 | 94.25 ± 0.18 |
| 19 | Ganges and Brahmaputra | 34.44 ± 0.05 | 44.09 ± 0.05 | 50.84 ± 0.10 | 58.34 ± 0.19 | 67.42 ± 0.19 | 71.52 ± 0.25 | 74.36 ± 0.27 | 81.68 ± 0.31 | 91.92 ± 0.28 |
| 20 | Yangtze | 55.94 ± 0.05 | 63.88 ± 0.05 | 68.99 ± 0.14 | 73.56 ± 0.11 | 80.09 ± 0.17 | 82.63 ± 0.11 | 84.74 ± 0.26 | 89.47 ± 0.22 | 95.63 ± 0.28 |
| 21 | Murray Darling | 23.38 ± 0.03 | 33.83 ± 0.04 | 41.45 ± 0.09 | 49.57 ± 0.25 | 61.47 ± 0.25 | 65.99 ± 0.31 | 69.30 ± 0.30 | 77.80 ± 0.53 | 90.21 ± 0.51 |
| 22 | Huang He | 46.85 ± 0.09 | 58.85 ± 0.02 | 67.29 ± 0.07 | 73.59 ± 0.17 | 80.94 ± 0.06 | 84.16 ± 0.43 | 86.31 ± 0.27 | 90.49 ± 0.05 | 96.16 ± 0.22 |
| 23 | Indus | 47.60 ± 0.08 | 56.50 ± 0.03 | 62.00 ± 0.05 | 67.78 ± 0.28 | 75.09 ± 0.16 | 78.21 ± 0.18 | 80.50 ± 0.15 | 86.27 ± 0.28 | 93.60 ± 0.46 |
| 24 | Euphrates and Tigris | 39.06 ± 0.08 | 48.00 ± 0.04 | 55.25 ± 0.15 | 62.51 ± 0.22 | 70.98 ± 0.13 | 74.93 ± 0.26 | 77.73 ± 0.35 | 84.79 ± 0.33 | 93.68 ± 0.54 |
| 25 | Danube | 49.22 ± 0.04 | 58.86 ± 0.07 | 64.84 ± 0.10 | 71.02 ± 0.21 | 78.36 ± 0.21 | 81.37 ± 0.18 | 83.28 ± 0.31 | 88.33 ± 0.22 | 94.98 ± 0.27 |
| 26 | Orange | 31.72 ± 0.02 | 41.43 ± 0.23 | 48.67 ± 0.12 | 55.43 ± 0.23 | 64.69 ± 0.30 | 69.30 ± 0.42 | 73.17 ± 0.45 | 81.34 ± 0.46 | 91.16 ± 0.29 |





HESSD
9, 6615–6647, 2012



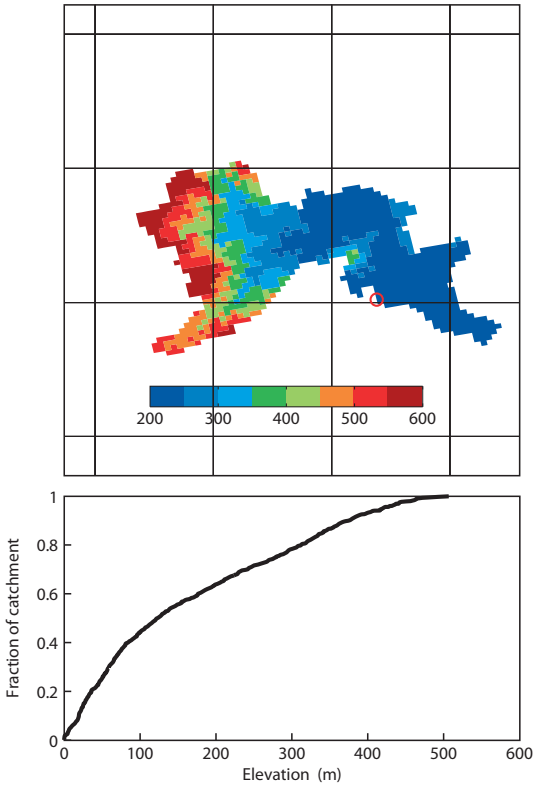


**Fig. 1.** Illustrating the sub-grid parameterization. The coarse grid on the top figure represents the 25 km × 25 km cells. The catchment elevation map is shown on a 1 km × 1 km grid. The outflow is indicated by a red circle. The river routing properties for the cell with this outflow are derived from the 1 km × 1 km grid. Such a property is shown in the bottom plot in which elevation vs catchment fraction is plotted.





HESSD
9, 6615–6647, 2012



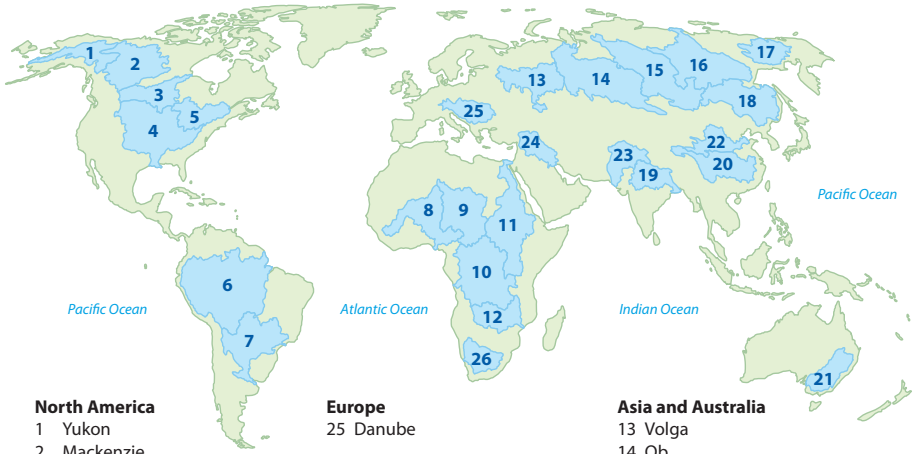


**Fig. 2.** Major Worlds River Catchments (reproduced from UNEP; WCMC; WRI; AAAS; Atlas of Population and Environment, 2001).





HESSD
9, 6615–6647, 2012



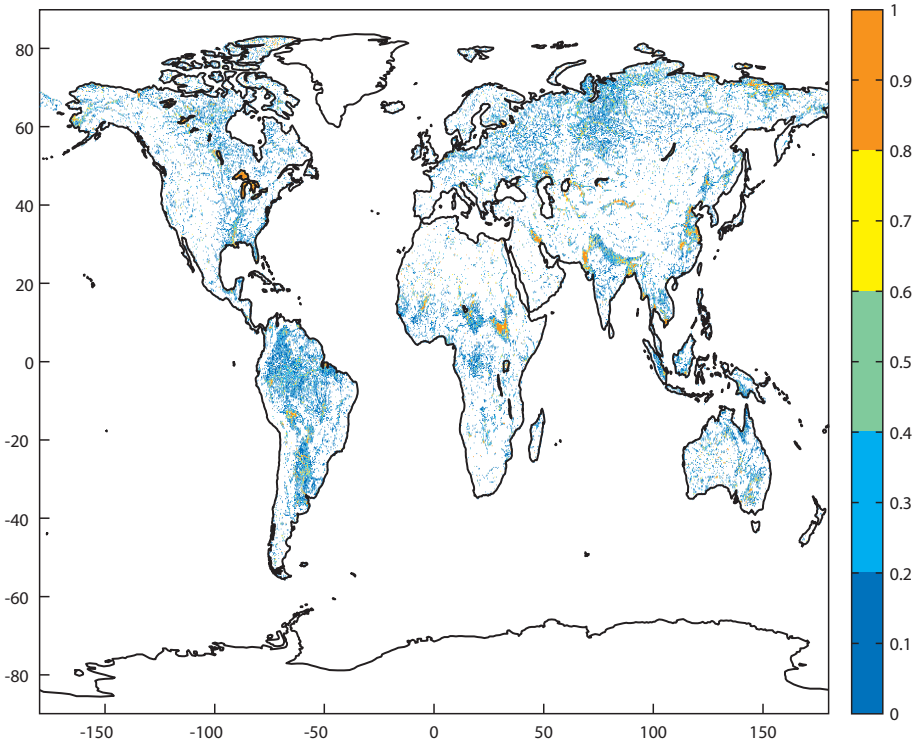


**Fig. 3.** Fractional coverage of flooding of 25 km by 25 km cells. 1 means that the cell is flooded to 100 %, 0.5 means that the area within the cell is flooded to 50 % and 0 means that the area is not flooded at all. The figures shows the 50 yr return period.





HESSD
9, 6615–6647, 2012



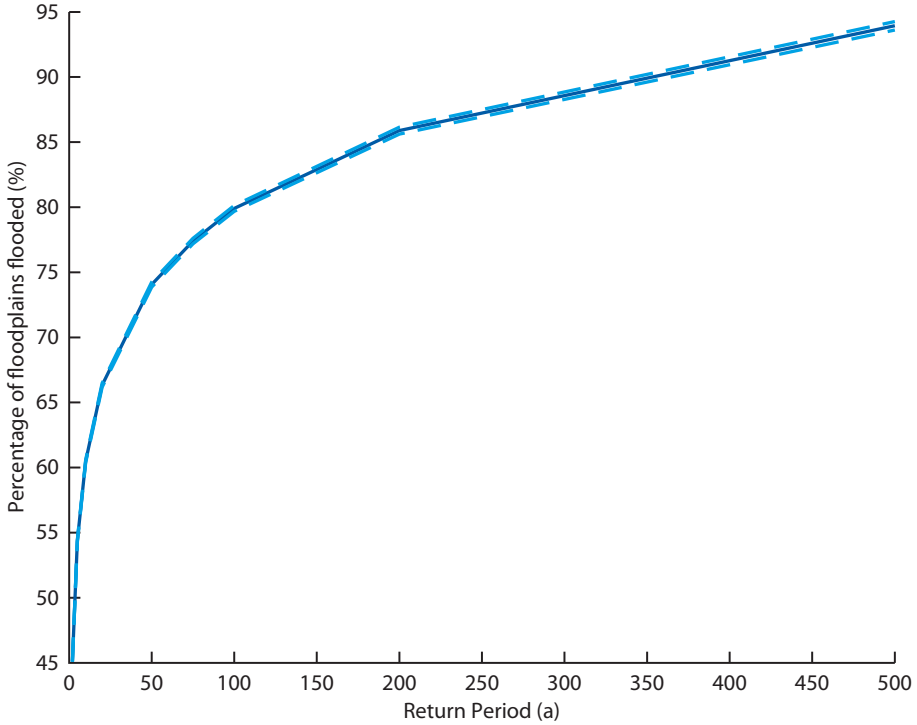


**Fig. 4.** Average flooded area of the largest 20 catchments. The 5th and 95th percentile derived from the estimation of the Gumbel distribution is displayed as dotted lines.





HESSD
9, 6615–6647, 2012



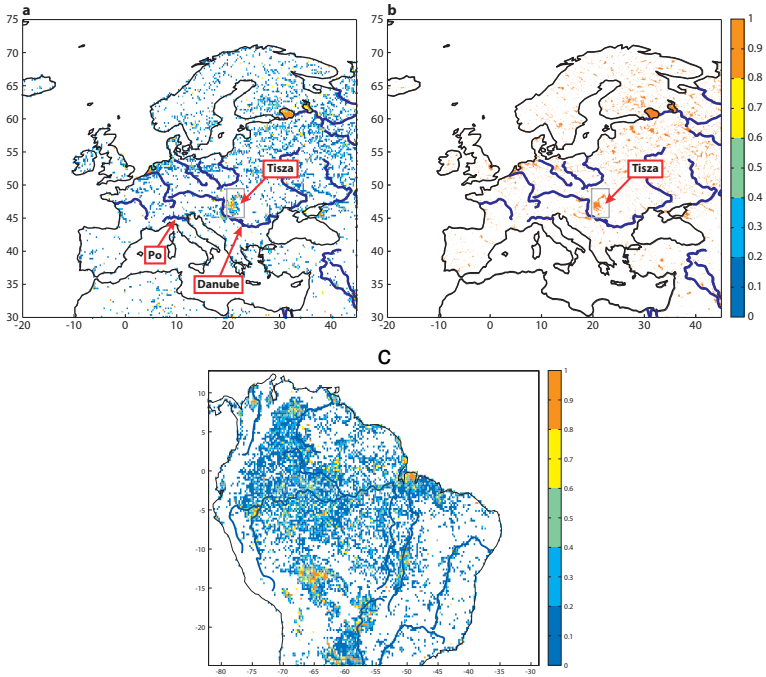


**Fig. 5. (a)**: fractional coverage of flooding of 25 km by 25 km cells for a 50 yr return period focusing on Europe only. 1 means that the cell is flooded to 100 %, 0.5 means that the area within the cell is flooded to 50 % and 0 means that the area is not flooded at all. Major European rivers are shown as blue lines. **(b)**: flooding of 1 km by 1 km cells for a 50 yr return period focusing on Europe only (binary map). Major European rivers are shown as blue lines. **(c)**: fractional coverage of flooding of 25 km by 25 km cells for a 50 yr return period focusing on South America only. 1 means that the cell is flooded to 100 %, 0.5 means that the area within the cell is flooded to 50 % and 0 means that the area is not flooded at all.





HESSD
9, 6615–6647, 2012



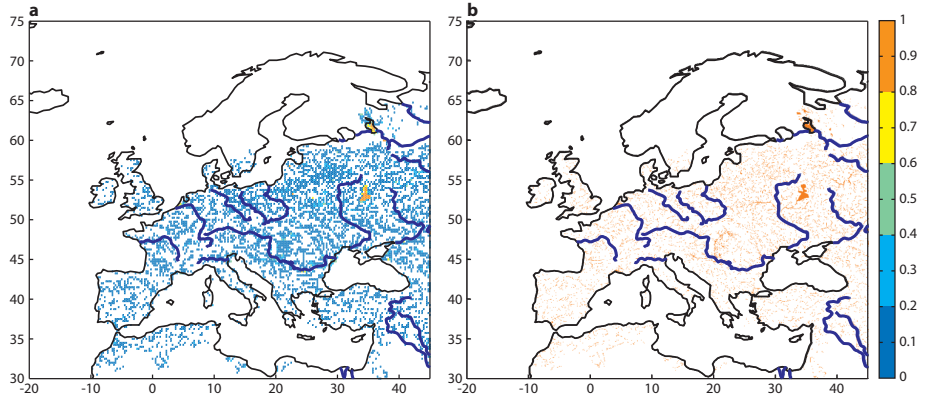


**Fig. 6. (a)**: fractional coverage of flooding of 25 km by 25 km cells for the benchmark data set focusing on Europe only. 1 means that the cell is flooded to 100 %, 0.5 means that the area within the cell is flooded to 50 % and 0 means that the area is not flooded at all. Scandinavia contains no data in this data set. Major European rivers are shown as blue lines. **(b)**: flooding of 1 km by 1 km cells for a 50 yr return period focusing on Europe only (binary map) for the Benchmark data set. Scandinavia contains no data in this data set. Major European rivers are shown as blue lines.





HESSD
9, 6615–6647, 2012



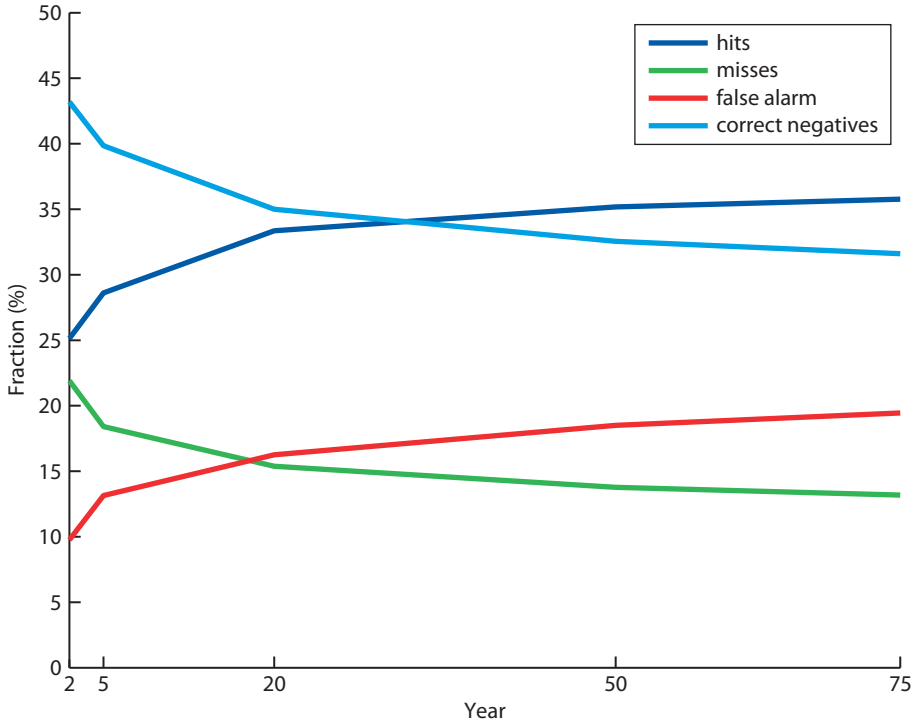


**Fig. 7.** Comparison of percentage of hits, misses, false alarms and correct negatives (definition in Table 1) for the 20 largest catchments on the globe and different return periods (areas which contain no data in the benchmark are masked). This compares the maps computed in this study to the data of the benchmark study.





HESSD
9, 6615–6647, 2012



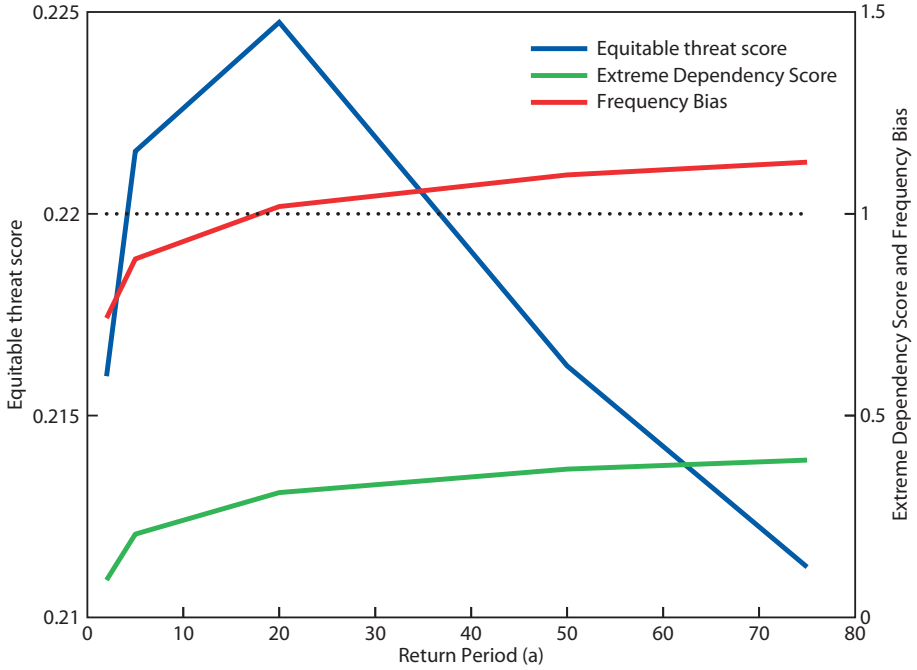


**Fig. 8.** Equitable Threat Score of different return periods with a benchmark model as "observations". An ETS of larger than 0 is skilfull and the higher values are better.





HESSD
9, 6615–6647, 2012